

**UCSF**

**UC San Francisco Electronic Theses and Dissertations**

**Title**

Longitudinal changes in brain structure and integrity during acute HIV

**Permalink**

<https://escholarship.org/uc/item/1z7432sn>

**Author**

Tsuei, Torie

**Publication Date**

2019

Peer reviewed|Thesis/dissertation

Longitudinal changes in brain structure and integrity during acute HIV

by  
Torie Tsuei

THESIS  
Submitted in partial satisfaction of the requirements for degree of  
MASTER OF SCIENCE

in  
Biomedical Imaging

in the  
GRADUATE DIVISION  
of the  
UNIVERSITY OF CALIFORNIA, SAN FRANCISCO

Approved:

DocuSigned by:  
*Victor Valcour* Victor Valcour  
50F20E448E7C48F... Chair

DocuSigned by:  
*Yann Cobigo* Yann Cobigo

DocuSigned by:  
*Duygu Tosun* Duygu Tosun

DocuSigned by:  
*Maria Luisa Gorno Tempini* Maria Luisa Gorno Tempini  
8A46C9EF252D4F2...

---

Committee Members

Copyright 2019  
by  
Torie Tsuei

# Acknowledgements

None of this work would have been possible without the guidance and expertise of Dr. Victor Valcour along with his initial vision of the SEARCH imaging study. I would like to express my sincerest gratitude to Dr. Yann Cobigo for his consistent mentorship and support, along with members of the MAC Imaging Core and the Valcour Lab for their valuable insights. I would also like to extend my appreciation to Dr. Isabel Allen for her statistical acumen and enthusiasm. In addition, I would like to thank my committee members Dr. Dugyu Tosun-Torgut and Dr. Maria Luisa Gorno Tempini for their guidance and constructive feedback. Finally, I am grateful for my friends and family for providing me with encouragement and the opportunity to pursue my ambitions.

# Longitudinal changes in brain structure and integrity during acute HIV

by

Torie N. Tsuei

## **Abstract**

Cognitive impairment persists in the form of HIV-associated neurocognitive disorder (HAND) among chronically infected individuals despite successful viral suppression. Widespread access to combination antiretroviral therapy (cART) has allowed infected individuals to initiate treatment at an earlier time point and effectively reduce the risk of HIV-related mortality and morbidity. The current study examines whether cART, when initiated within days to weeks following infection, can longitudinally preserve brain health. Quantitative magnetic resonance image (MRI) methodologies were used to analyze T<sub>1</sub>-weighted structural images and diffusion tensor imaging (DTI) metrics. Specifically, region of interest and voxel-wise volume and tensor-based spatial statistics (TBSS) approaches were performed to evaluate differences in brain volumes and white matter microstructure. We examined 31 acute HIV (AHI) participants who had paired month 0 (baseline) and month 24 (two-year follow-up) scans. Participants were comparatively analyzed in both a longitudinal manner to themselves, and a cross-sectional manner against 25 healthy control (CO) participants. As an indication of inflammation, CD8 t-lymphocyte counts was examined as a clinical covariate. The 31 AHI participants had a median (IQR) age of 26 (23-30) years at the time of enrollment and a median (IQR) baseline CD4 count of 576 (370-868) cells/ $\mu$ L. All immediately initiated cART. The 25 healthy controls had a median (IQR) age of 31 (26-37) years. Differences of brain integrity in the AHI group followed longitudinally were

observed. Baseline CD8 count was significantly associated with increased mean diffusivity (MD) in the longitudinally infected, present in the genu and the splenium of the corpus callosum, the corona radiata, and the superior longitudinal fasciculus (all  $p < 0.05$ ). Structural analysis revealed enlarged corpus callosum ( $p < 0.01$ ) volumes, as well as enlarged caudate and thalamus subcortical gray matter volumes in the longitudinally infected AHI participants (both  $p < 0.05$ ). Differences of brain integrity in the AHI group after 24 months of treatment were observed compared to healthy controls. Specifically, fractional anisotropy (FA) was reduced in AHI at 24 months compared to controls in models adjusting for age in the corpus callosum, the corona radiata, and the left superior longitudinal fasciculus (all  $p < 0.05$ ). Structural analyses revealed enlarged putamen and the caudate volumes (both  $p < 0.05$ ). We conclude that differences in both brain integrity and structural volumes can be seen in AHI with successful viral suppression when compared to healthy controls. Future work will include longitudinal imaging data from healthy controls who are followed over two-year follow-up to ensure that observed changes are disease specific. We will also comparatively investigate longitudinally treated chronic HIV-infected participants ('positive controls') to examine if the differences are similar to those seen when therapy is initiated in the chronic stage of infection. We will examine inflammatory plasma and CSF biomarkers to inform potential mechanisms and, separately, cognitive testing to inform clinical significance.

# Table of Contents

<b>1. Introduction</b>	<b>1</b>
1.1. HIV, Cognition, and Brain Injury	1
1.2 Acute HIV	2
1.3 Diffusion Tensor Imaging in HIV Infection	2
1.4 Study Aims	4
<b>2. Methods</b>	<b>5</b>
2.1 Principles of Diffusion	5
2.2 Study Design	7
2.3 Image Acquisition	8
2.4 Image Processing	9
2.5 Conjugate Analyses of Spatial Normalization	12
2.6 Statistical Approaches	13
<b>3. Results</b>	<b>17</b>
3.1 Clinical and Demographic Characteristics	17
3.2 Longitudinal Changes in Acute HIV	19
3.3 Changes by Disease State: Healthy Controls vs. HIV Infected at 24 months	21
3.4 Sensitivity Analysis	23
<b>4. Discussion</b>	<b>25</b>
4.1 Major Findings	25
4.2 Clinical Interpretations	26
4.3 Exploratory Findings	28
4.4 Limitations and Future Aims	29
<b>5. Conclusion</b>	<b>31</b>

# List of Figures

Figure 1: B-value function	5
Figure 2: Longitudinal voxel-wise analysis	19
Figure 3: Disease state voxel-wise analysis	22
Figure 4: Compartmentalized diffusive motion	27



# List of Tables

Table 1: Demographic and clinical variables	18
Table 2: Structural ROI analysis	20
Table 3: Structural ROI analysis effect sizes	20

# **1. Introduction**

## **1.1. HIV, Cognition, and Brain Injury**

Southeast Asia contains the second most prevalent population in the world of people living with human immunodeficiency virus (HIV) infection.<sup>1</sup> In addition to compromising the immune system and causing opportunistic infection, HIV, itself, is known to have neuropathogenic properties.<sup>2</sup> These pathogenic properties are the core of current challenges, wherein people living with HIV who have never had opportunistic infections and have access to the best available therapies continue to experience cognitive impairment. In the chronic stage of infection, up to 50% of people living with HIV have neuropsychological testing impairment meeting research criteria for HIV-associated neurocognitive disorder (HAND).<sup>3</sup> Still, some infected individuals maintain preserved brain function even into later stages of disease.<sup>4-6</sup> Identifying neuro-preserving factors is of high clinical relevance.

In recent decades, widespread access to combination antiretroviral therapy (cART) has allowed infected individuals to live with a markedly reduced risk for opportunistic infections, and has reduced the prevalence of severe forms of HAND as well as overall HIV-related morbidity and mortality.<sup>7-10</sup> Given that not all individuals experience brain changes in the setting of HIV, there is great clinical interest and public health incentive to identify if very early cART initiation maintains brain health. There are currently no data to inform whether the earliest initiation of therapy is brain protective, leading us to examine brain changes following treatment initiated during the first weeks of infection by leveraging a novel cohort from Bangkok, Thailand.

## **1.2 Acute HIV**

Acute HIV infection (AHI) describes the earliest period following initial viral exposure, and typically lasts around four weeks.<sup>11,12</sup> During this period, the virus can cross the blood-brain barrier, and is associated with brain inflammation before plasma HIV antibodies and, sometimes, systemic and central nervous system (CNS) symptoms are identifiable.<sup>13</sup> AHI is considered the earliest stage of HIV infection and is compared to primary HIV (PHI, <1 year of infection but after plasma antibodies are present) and chronic HIV (CHI, >1 year of infection). Neuroimaging studies demonstrate brain atrophy, as well as changes in brain integrity, inflammation, and metabolism during the chronic stage of HIV.<sup>14</sup> Previous studies report brain inflammation by magnetic resonance spectroscopy (MRS) in AHI individuals prior to treatment, as well as the reduction of selected structural volumes over two years following treatment initiated during AHI (i.e. putamen atrophy), although comparative groups of uninfected controls were not available.<sup>15,16</sup> Our prior work did not identify DTI abnormalities among study participants imaged during AHI before treatment, suggesting that early treatment may be protective.<sup>17,18</sup>

## **1.3 Diffusion Tensor Imaging in HIV Infection**

In groups of people where chronic HIV infection has been successfully suppressed with cART (>45 years old), investigators continue to find cognitive impairment, gray matter atrophy, and widespread white matter microstructural abnormalities.<sup>19</sup> Previous structural region of interest (ROI), connectivity, and voxel-wise analyses in samples of chronically infected individuals demonstrated reduced nodal inefficiency, fiber integrity, and compromised frontal/motor regions.<sup>20-22</sup> Nodal efficiency is a graph theory measure derived from structural connectivity analysis that may measure information processing capabilities. Fiber integrity reduction refers to the observed reduction in fractional anisotropy (FA) and increased mean diffusivity (MD) metrics.

The etiology of these abnormalities is less clear and may be due to host-inflammatory responses.<sup>23</sup> These studies are also unable to differentiate if the abnormalities are due to active processes or a hallmark of injury occurring during the years before successful treatment with cART, since most such study participants would have initiated therapy only when immune compromise was seen. Although, in more recent years, study participants may have been started on therapy upon diagnosis, reflecting changes in treatment recommendations, this still would likely be months to years given known delays in HIV diagnosis and access to care and since, during this time, HIV may be relatively asymptomatic.

Brain regions of interest (ROIs) recognized as vulnerable in chronic HIV include the corpus callosum, caudate, putamen, thalamus, and hippocampus.<sup>24,25</sup> Prior neuroimaging analyses from our research group has shown longitudinal reduction in brain volume of AHI participants, evidence supportive of brain atrophy in the putamen as well as the caudate at rates that were out of proportion to that anticipated from published work on healthy controls; however, co-enrolled controls were not then available for direct comparisons.<sup>16</sup>

Since the initiation of cART during the chronic phase of HIV does not appear to be fully neuroprotective against HAND, it is of particular interest to determine if initiation at an earlier time point, prior to structural deficit and cognitive decline, can be protective against neurological disease progression. Of particular note, DTI can be helpful in assessing white matter structural integrity of treated individuals at various time points following initiation of cART during AHI. Although our prior study did not identify DTI abnormalities in AHI, previous studies among individuals with primary HIV, some who had brief exposure to cART, identified higher FA and lower mean and radial diffusivity (RD) in the corpus callosum and corona radiata.<sup>24</sup> Thus, it is of

particular interest to investigate whether the very earliest administration of cART during AHI may prevent neuropathogenic developments.

#### **1.4 Study Aims**

The current project will examine the evolution of white matter microstructural change over two years among individuals with initiation of cART during AHI. We will examine changes in DTI and structural volumes over 24 months by comparing individuals' baseline and two-year follow-up image data to each other. Structural regions of interest (ROIs), chosen based on published literature in CHI and previous work by our group, will be investigated. We will also complete voxel-wise DTI and structural analyses to explore more broadly if abnormalities emerge in other brain regions.<sup>24,25</sup> Additionally, we will compare AHI cases at two-year follow-up to healthy controls.

Should we identify abnormalities in AHI at 24 months, this study will then examine baseline biological parameters correlative to progressive brain injury in successfully suppressed AHI individuals. This study has public health relevance if we demonstrate generally preserved microstructural integrity associated with early treatment as it will contrast that of the published literature among individuals treated in later stages of disease. These proposed findings would support efforts for initiation of cART as early as possible, a guidance that has not yet achieved international consensus. Should abnormalities be found, our work would suggest the need for adjuvant therapies for neuroprotection.

## 2. Methods

### 2.1 Principles of Diffusion

Diffusion tensor imaging (DTI) is a nuclear magnetic resonance imaging (MRI) technique that measures signal attenuation based on the principles of Brownian motion in a restricted environment, and involves acquisition of diffusion images in multiple non-collinear directions. In the brain, DTI is used to noninvasively characterize white matter tract orientation and quantify microstructural integrity from acquired  $T_2$ -weighted images with spatial accuracy.<sup>26</sup>

Mono-exponential signal attenuation captured in acquired  $T_2$ -weighted images varies depending on a predetermined b-value ( $s \cdot mm^{-2}$ ), and contributes to the approximation of the macroscopic apparent diffusion coefficient constant (ADC) value. The b-value is a user-defined scalar factor that considers how adjustments in pulsed gradient parameters affect detection of changes in particle precession frequency (**Figure 1**).

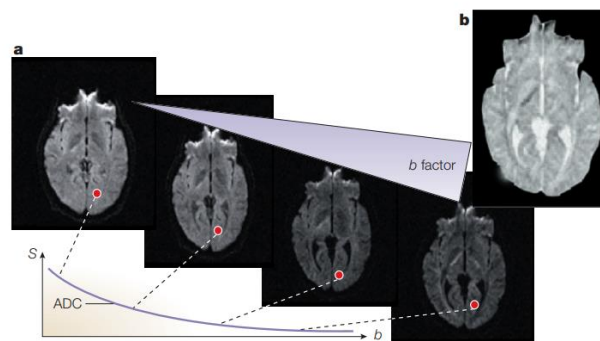


**Figure 1:** Differential b-values capture signal attenuation modulated by the diffusion coefficient. Increasing b-values will strengthen signal attenuation and improve image contrast.<sup>27</sup>

Such changes describe the phenomenon of incomplete signal refocusing due to changes in particle position, and ultimately influence subsequent signal attenuation, or measured diffusion. Pulsed gradients are cumulatively described by the b-value. The b-value accounts for the magnitude ( $G - T \cdot mm^{-1}$ ), duration ( $\delta - s$ ), and temporal spacing ( $\Delta - s$ ) between pulsed gradients

applied during diffusion image acquisition (**Equation 1**).  $\gamma$  ( $\text{rad}\cdot\text{s}^{-1}\cdot\text{T}^{-1}$ ) represents the gyromagnetic ratio of protons, and is squared along with magnitude and duration to account for both pulsed gradients. A fractional duration component is subtracted from temporal spacing, which represents periods of transitory slew rate and subsequent non-maximum gradient magnitude.

$$b = (\gamma G \delta)^2 \left( \Delta - \frac{\delta}{3} \right) \quad (1)$$

Adequately chosen b-values depend on systemic application. For example, a b-value ranging from 1000-1500  $\text{s}/\text{mm}^2$  is typically used when imaging the adult brain, while a b-value of 600-900  $\text{s}/\text{mm}^2$  is typically used to image the pre-adolescent brain. Generally, higher b-values are more sensitive to restrictive diffusion and result in better image contrast; tissues with random, molecular de-phasing experience greater signal loss, while restricted tissues that hinder random motion remain visually conspicuous.

Diffusion in biological tissues is constrained by cellular membranes, leading to anisotropic flow. Water in the CNS follows curvatures parallel to axonal fiber orientations, but movement is highly restricted in the directions perpendicular to white matter fibers. An effective diffusion tensor ( $D^{\text{eff}} - \text{mm}^2\cdot\text{s}^{-1}$ ) thus quantitatively relates the macroscopic proton concentration gradient ( $C - \text{mm}^{-3}$ ) and their diffusive flux ( $J - \text{mm}^{-2}\cdot\text{s}^{-1}$ ) in an anisotropic environment (**Equation 2**).

$$\mathbf{J} = -\mathbf{D}^{\text{eff}} \mathbf{C} \quad (2)$$

$D^{\text{eff}}$  elements represent three-dimensional proton displacement in the CNS along axonal bundles. Diagonalization of  $D^{\text{eff}}$  aligns the framework from native space into tensor eigenspace. The resulting eigenspace consists of eigenvalues and eigenvectors that correspond to diffusive motion captured along the principle directions of proton flow in a single voxel, and can be visualized as effective diffusion axes of an ellipsoid defining restricted water movement.<sup>28</sup> A

commonly used DTI measure is fractional anisotropy (FA), which assesses general diffusion asymmetry within a voxel. Another common DTI measure is mean diffusivity (MD), which describes diffusive changes recorded between the application of constant, pulsed gradients in the sequence paradigm by considering both radial (perpendicular) diffusivity (RD) and axial (parallel) diffusivity (AD).<sup>26</sup>

## 2.2 Study Design

Included study participants enrolled after seeking HIV testing and receiving AHI diagnosis at the Thai Red Cross AIDS Research Center's anonymous volunteer counseling and testing (VCT) clinic in Bangkok, Thailand (**Table 1**). Enrolled participants consented to neuroimaging, laboratory assessments, and clinical follow-up as outlined in a broader protocol for investigation of immunology and virology in AHI (SEARCH 010/RV 254).<sup>11</sup> Estimated duration of infection before cART initiation was calculated from participants' self-reported exposure date, or by taking the median date of multiple potential exposure dates. In this prospective study, preliminary analyses were performed to compare imaging of AHI participants at baseline to all follow-up scans collected after at least one year (i.e. month 12, month 18, and month 24 follow-up) with >90% collected at a 24 month time point.

Specifically, we examined all SEARCH 010/RV 254 participants who consented to and underwent neuroimaging on a 3.0 Tesla MRI (acquisition dates: 8/26/15–2/26/19). Several clinical and laboratory variables captured both at baseline and latest follow-up, including CD4 t-lymphocyte counts, CD8 t-lymphocyte counts, calculated CD4/CD8 ratio, and plasma HIV RNA (copies/mL), were also considered. MRI for the AHI group was performed following cART initiation in 26% of AHI participants (i.e. one to four cART doses received, MRI collected after



an average of two days), and were acquired at subsequent month 12, month 18, and month 24 follow-up time points.

### *Exclusion Criteria*

Participants were excluded from this study if they had concurrent positive serology for syphilis (serum VDRL) at baseline or follow-up. Although the SEARCH study has been collecting AHI participant scans on the 3.0 Tesla Philips Ingenia (n=138), individuals who did not have paired month 0 baseline and month 24 follow-up scans were excluded (n=98). Individuals were also excluded if motion and artifacts affecting image quality were present at either month 0 baseline or month 24 follow-up time points (n=9).

### **2.3 Image Acquisition**

All structural magnetic resonance imaging (MRI) data were acquired on the same Philips Ingenia 3T MRI scanner. A 15-channel phased array head coil was used for signal excitation and reception. High-resolution, three-dimensional, T<sub>1</sub>-weighted structural images were acquired using a turbo field echo (T<sub>1</sub>W 3D TFE) sequence (TR=8.1ms, TE=3.7ms, flip angle=8°, field of view (FOV)=256mm×256mm, voxel size=1mm×1mm×1mm, 165 slices with no gap). Diffusion weighting imaging sequences included gradients applied in 32 directions with a b-value of 1000 s/mm<sup>2</sup> (TR=11000ms, TE=111ms, flip angle=90°, FOV=256mm×256mm, slice thickness=2mm, 2380 axial slices). In the acquisition paradigm, two equally weighted, time-dependent pulsed gradients were implemented in conjunction with a conventional spin-echo (SE) sequence. The first gradient pulse was applied following the initial SE 90° pulse that generates free induction decay (FID) to represent phase coherence prior to diffusive movements. The second gradient pulse was applied after the SE 180° inversion pulse in order to capture incomplete refocusing of diffusive nuclei spins that had since moved from original recorded positions. In short, pulsed gradients were

used to detect and visualize subtle changes in water movement as differences in signal intensity, or signal attenuation.<sup>29</sup>

## **2.4 Image Processing**

### *Hybrid Temporal Processing*

Both cross-sectional and longitudinal analyses were used to process a group of individuals with variable imaging time points. All longitudinal diffusion and structural images, including every time point collected for included AHI participants (month 0, month 12, month 18, and month 24) initially underwent longitudinal analyses, described in the following sections, and output a group template. All images collected at month 0 baseline, including CO and AHI participants, were then processed in a cross-sectional manner using the group template built from longitudinal analysis. Iterative group template creation in cross-sectional analyses was suppressed such that included images were simply warped into initial target template space, but did not contribute to building a new cross-sectional-specific group template. This ensured that a single group template from hybrid processing could be implemented in comparative statistical analyses.

### *DTI Longitudinal Image Processing*

Diffusion images were visually inspected and denoised, and images with significant artifacts were excluded from further analysis.<sup>30</sup> The FSL MCFLIRT algorithm was used to register diffusion images to the primary volume of the sequence.<sup>31</sup> Data reflecting absolute displacement parameters beyond 1mm were screened out, and volumes surpassing relative displacement parameters beyond 1mm were removed. Background voxels not considered to be brain tissue were then masked out of the diffusion image volumes by applying a median otsu function.<sup>32</sup> This function utilized the  $B_0$  acquisitions to provide a mask using otsu thresholding with a 4mm radius

and four iterations to minimize intra-class variance.<sup>33</sup> Re-aligned diffusion images, corresponding masks, b-vectors, and b-values were used to correct for eddy current-induced distortions.<sup>34</sup>

Remaining tensor eigenvalues were then fitted using the Diffusion Imaging in Python package (DIPY) with a non-linear least-squares approach derived fitting model to construct FA, MD, RD and AD maps.<sup>35</sup> Post processing steps included construction of a group template and normalization of DTI tensors into standard Diffusion Tensor Imaging – Tool Kit (DTI-TK) space. Voxels with significant signal outliers, which degrade template generation and are identified as voxels with tensor norm value greater than 100, were first masked out of the tensor maps. Tensor Based Registration was completed using DTI-TK. A diffusion tensor group template specific to the Thailand population was created in a previous study, and was used as a target to build the group template using tensor-based registration. Specifically, participants' DTI tensors were processed through a bootstrapping algorithm to a standard DTI template provided by DTI-TK. The next step involved computing affine alignment transformations using DTI-TK to place all participants' tensors into standard space with a normalized mutual information cost function implemented over three iterations. A binary mask was then created using the trace of the diffusion tensor (MD) map to mask out tensors outside template brain tissue. A final deformable alignment was then used to register all participants to iteratively refine the Thai group template.

The stored affine transformations and displacement field vectors were then composed into a global displacement field and applied to transform the native participant DTI volumes to standard Thai group template space to minimize interpolation steps. Analyses followed conventional tract based spatial statistics (TBSS) integration pipeline using FSLtools in DTI-TK space. After the post processing steps were completed, proceeding skeleton creation, projection and statistics were carried out using standard FSL TBSS processing (FMRIB Software Library;

<http://fsl.fmrib.ox.ac.uk/fsl/fslwiki/TBSS>). Skeletonised FA maps were created to eliminate the locational variability of tracts by projecting individuals' voxels of maximum anisotropy onto a group template skeleton for registered statistical comparison.

### *Structural Longitudinal Image Processing*

Before image pre-processing, all T<sub>1</sub>-weighted images were visually inspected for quality control and images with excessive motion or image artifact were excluded. T<sub>1</sub>-weighted images underwent bias field correction using N3 algorithm, and segmentation was performed using SPM12 Unified Segmentation (Wellcome Trust Center for Neuroimaging, London, UK, <http://www.fil.ion.ucl.ac.uk/spm>).<sup>36</sup> An intra-subject template was created using a composition of non-linear diffeomorphic and rigid-body registration drawn from symmetric diffeomorphic registration methods implemented in a longitudinal MRI framework.<sup>37</sup> The intra-subject template was also segmented using SPM12's Unified Segmentation.

A within-participant modulation was applied by multiplying each time points' Jacobian matrix with intra-subject averaged tissues.<sup>38</sup> A group template was generated from the within-subject average gray and white matter tissues (GM, WM) as well as the CSF by non-linear registration template generation using the geodesic shooting algorithm.<sup>39</sup> Modulated intra-subject GM and WM were normalized and smoothed at 10mm full width half maximum Gaussian kernel in the group template. Every step of the transformation was carefully inspected from the native space to the group template. For statistical purposes, linear and non-linear transformations between the group template space and International Consortium of Brain Mapping (ICBM) were applied.<sup>40</sup>

## 2.5 Conjugate Analyses of Spatial Normalization

Parametric mapping of brain regions from T<sub>1</sub>-weighted structural images was performed through a composition of linear and non-linear registrations into a common template using diffeomorphic mapping. Diffeomorphic mapping captures individual tensor element displacement within a given neighborhood in an optimization metric to generate smoothed displacement fields.<sup>41</sup> As a result, every element was uniquely interpolated to best fit the group template. Structural diffeomorphism involves zero order tensors (structural maps), whereas diffusion tensor mapping involves second order tensors. Both methods belong to a larger framework: Large Deformation Diffeomorphic Metric Mapping (LDDMM). Voxel-based morphometry (VBM) and TBSS minimized spatial inconsistencies among included participants such that group difference analyses may be achieved through voxel-wise coherence. In this study, both methods were implemented to investigate longitudinal differences in brain volumetric and regional fiber integrity, respectively.

### *Comparison of Tissue Volume and Densities with Voxel-Based Morphometry (VBM)*

VBM is an image processing technique used for group comparison of brain matter volume and density through analysis of T<sub>1</sub>-weighted structural images. VBM is limited, however, by a loss of information due to smoothing, which is performed to estimate voxel-wise similarity among geometrically variant participants. This analysis contributed to comparisons between larger groups of voxels in complete ROIs and whole brain analysis.

### *Tensor Normalization and Tract Comparison with Tract-Based Spatial Statistics (TBSS)*

Diffusion images require greater spatial focalization such that relative tensor geometries are not heavily interpolated. Subsequently, the realistic orientation of macroscopic tracts was altered to achieve spatial coherence for voxel-wise statistical analyses. TBSS, a diffusion image processing technique, optimizes analyses by projecting voxels with peak anisotropic values onto

an alignment-invariant tract mean FA skeleton, representing the center of all tracts common to the comparative groups. Projection of peak anisotropic values was done using carefully fine-tuned nonlinear registration, thereby reducing spatial smoothing and improving the objectivity and interpretability of tensor-based group comparison statistical models.<sup>42</sup>

## **2.6 Statistical Approaches**

DTI and conjugate structural metrics were investigated among three group comparisons. The first comparison structure explored the longitudinal changes between AHI at month 0, AHI (0), vs. AHI at follow-up time points. In voxel-wise and ROI structural analyses, comparison of single longitudinal time point, AHI at month 24, AHI (24), were investigated. A comparison of disease states was then performed to examine differences between healthy controls, CO vs. AHI (24).

### *Statistical Considerations*

Several clinical and laboratory measures were not available at the same time point as the MRI collection date; measures at longest follow-up were thus considered (month 12, month 18, and month 24) as representative covariates in comparative models of AHI (24) imaging metrics. One-way analysis of variance (ANOVA) testing was performed to assure that measures collected at the three longest follow-up time point groups did not significantly differ, and subsequently would not alter group comparison. Affected clinical measures included both CD4 t-lymphocyte counts ( $p>0.05$ ) and CD8 t-lymphocyte counts ( $p>0.05$ ), both of which showed insignificant differences among the three collection date groups. Several demographic variables were observed among the participant groups, including significant differences in age, sex, and education. Given the sample size, we chose appropriate covariates parsimoniously. Total intracranial volume (TIV) was used to adjust for collinear differences in sex.<sup>43,44</sup> Each demographic factor found to differ

across groups was initially adjusted for in every comparison structure to determine the most significant contributing covariates, which were retained. Voxel-wise models testing for baseline group differences were adjusted for age and TIV.<sup>45,46</sup> Structural ROI models testing for baseline group differences were adjusted by age, and ROI values were normalized by TIV to adjust for differences in sex.

#### *DTI Tract-Based Spatial Statistics and Voxel-Wise Analysis*

Skeletonised maps created with TBSS were used to perform voxel-wise analysis of DTI metrics. Voxel-wise statistical analyses was completed with FSL Randomise, which corrects for family-wise error (FWE) using 5000 permutations and threshold-free cluster enhancement (TFCE).<sup>47-49</sup> We chose this approach since voxel-wise statistical analyses probes group differences with finer spatial accuracies compared to region of interest (ROI) analysis, which represents entire regions as a single functional unit. Voxel-wise group differences in DTI metrics are examined across the whole brain, and provide a means to explore whether statistically significant differences persist after controlling for clinical covariates. Group differences were characterized using the Johns Hopkins University atlas (JHU) labels transformed in to the DTI-TK space. We focused on investigating JHU regions of interest (ROIs) drawn from previous methods in our group and existing HIV literature. *A priori* chosen ROIs included: the corpus callosum (genu, body, and splenium), known to exhibit reduced FA in early infection, the corona radiata (anterior, superior, and posterior), known to be affected in early and chronic HIV, and the superior longitudinal fasciculus (left, right), known to be affected in early HIV.<sup>17,24,25,50</sup>

#### *Structural Volumetric Based Morphometry and Voxel-Wise Analysis*

VBM was performed by smoothing images using FSL tools with a sigma 3mm Gaussian kernel as a mean filter. Voxel-wise statistical analyses were computed on both gray (GM) and

white matter (WM) tissues using FSL Randomise, which corrects for family-wise error (FWE) using 5000 permutations and threshold-free cluster enhancement (TFCE).<sup>47-49</sup>

### *Structural Region of Interest Analysis*

ROI analysis was implemented by warping the Desikan-Killiany Cortical Atlas into group template space using SPM12 deformation tools, using nearest neighbor interpolation to preserve regional integrity.<sup>39,51</sup> Advanced Normalization Tools (ANTs) ImageIntensityStatistics was then used to calculate regional volumes (in mm<sup>3</sup>) and masked by gray and white matter tissue probability maps (GM, WM). *A priori* chosen regions were chosen from previous methods in our group and existing HIV literature. In GM, the frontal lobe, temporal lobe, caudate, nucleus accumbens, cerebellum, hippocampus, and total cortical gray matter regions were investigated. In WM, the frontal lobe, temporal lobe, cerebellum, corpus callosum, and cerebral white matter regions were investigated. In addition, the pallidum, putamen, thalamus, and brainstem were analyzed as composite volumes, inherently consisting of both GM and WM tissues.<sup>24,52,53</sup> Cohen's  $d$  effect sizes were calculated to estimate the amount of observed differences in adjusted models.

### *Longitudinal analyses with Bayesian mixed linear effects model (BMLE)*

The group and participants' voxel-based trajectories of GM atrophy and the disruption of DTI indices (FA, MD) were longitudinally modeled using hierarchical Empirical Bayesian linear mixed-effects methods.<sup>38</sup> In brief, the model consists of two hierarchical levels: the single participant trajectory and the group trajectories. Trajectory is defined as a first-degree polynomial; the  $j$ -th time point of the subject  $i$  represents the volumetric intensity or the DTI metric in a single voxel  $y_{ij}$  (**Equation 3**).



$$y_{ij} = \sum_{d=0}^D \theta_{id}^{(1)} t_j^d + \epsilon_{ij}^{(1)} \quad (3)$$

A single voxel is fitted using a design matrix  $X^{(1)}$ , where  $t_j$  is the subject's age at the time point  $j$  acquisition day, and  $\theta^{(1)}$  and  $\epsilon^{(1)}$  represent the first level vector of parameters and noise, respectively. The complete model can be written as:

$$y = X^{(1)} \theta^{(1)} + \epsilon^{(1)} \quad (4)$$

$X^{(1)}$  and  $\epsilon^{(1)}$  define the first level design matrix and noise, respectively. The model's second level can be represented as:

$$\theta^{(1)} = X^{(2)} \theta^{(2)} + \epsilon^{(2)} \quad (5)$$

$X^{(2)}$ ,  $\theta^{(2)}$  and  $\epsilon^{(2)}$  are equivalent to the second level design matrix, parameters and noise, respectively. The second level design matrix also holds the explanatory variables of interest at baseline. At each level, the noise distribution is drawn from a centered Gaussian:  $\epsilon^{(u)} \sim N(0, C_\epsilon^{(u)})$ , where  $C_\epsilon^{(u)}$  is the hierarchical level  $u$  covariance matrix.

The chosen primary predictors of change included a measure of inflammation, CD8 t-lymphocyte counts at baseline. Time and the interaction between included CD8 counts at baseline and time provided the framework for assessing the impact of CD8 counts at baseline on rates of change in GM tissue volumes or DTI metrics.

### 3. Results

#### 3.1 Clinical and Demographic Characteristics

After quality control, 31 AHI participants (100% male, 55% completed at least a bachelor's degree) with a median (interquartile range, IQR) age of 26 (23-30) years at enrollment, and 25 HIV-uninfected control (CO) participants (52% male, 0% completed at least a bachelor's degree) with a median (IQR) age of 31 (26-37) years at enrollment were evaluated (**Table 1**). The AHI participants did not differ from control participants in age ( $p>0.05$ ); however, there were proportionally more females in the control group ( $p<0.01$ ) and differences in years of education were apparent ( $p<0.01$ ). CD4 t-lymphocyte counts of AHI and CO differed, as expected ( $p<0.01$ ), but did not differ between AHI participants and month 24 and CO, indicating immune reconstitution associated with cART. The median (IQR) estimated infection duration prior to cART initiation was 18 (14-22) days. Antiretroviral regimen differed between AHI participants at month 0 vs. month 24 since a subset of participants (52%) switched from Efavirenz (EFV-based) to Dolutegravir (DTG-based) treatments in accordance with the parent protocol and changing international recommendations. Most AHI participants were classified into early Fiebig Stages (I-III, 87%). This group of early Fiebig stage participants had lower CD4/CD8 ratios (1.09 (0.52) vs. 1.31 (0.31)) and lower plasma  $\log_{10}$  HIV RNA (5.66 (1.37) vs. 6.09 (1.14)) compared to AHI individuals classified into late Fiebig Stages (IV-V) at enrollment.

**Table 1:** Demographic and clinical variables of acute HIV (AHI) and healthy control (CO) participants.

	AHI at Month 0 (Baseline)	AHI at Month 24 (Follow-Up)	CO	p-value (AHI vs. CO)
Number of participants	31	31	25	
Age in years, median (IQR)	26 (23-30)	-	31 (26-37)	0.10
Sex, n (%) male	31 (100%)	-	13 (52%)	<0.01
Education in years, median (IQR)	22 (18-22)	-	15 (15-18)	<0.01
CD4 in cells/ $\mu$ L, median (IQR)	405 (267-505)	778 (643-945) <sup>a</sup>	879 (689-1057)	<0.01 & 0.14 <sup>b</sup>
CD8 in cells/ $\mu$ L, median (IQR)	576 (370-868)	732 (502-929) <sup>a</sup>	612 (457-1002)	0.47 & 0.11 <sup>b</sup>
CD4/CD8 ratio, median (IQR)	0.64 (0.42-1.32)	1 (0.81-1.42) <sup>a</sup>	1.53 (0.97-1.76)	<0.01 & 0.01 <sup>b</sup>
PHQ9 composite score, median (IQR)	8 (6-12)	7 (3-11) <sup>c</sup>	3 (1-8)	<0.01 & 0.01 <sup>b</sup>
Hospital ANX composite score, median (IQR)	11 (8-15)	6 (4-12) <sup>c</sup>	6 (4-9.5)	<0.01 & 0.28 <sup>b</sup>
cART Regimen				
Efavirenz (EFV-based), n (%)	17 (55%)	1 (3%)	-	-
Dolutegravir (DTG-based), n (%)	14 (45%)	30 (97%)	-	-
Administered cART before MRI, n (%)	8 (26%)	-	-	-
Fielig Stage at Enrollment				
Early Stage (I-III), n (%)	27 (87%)	-	-	-
Late Stage (IV-V), n (%)	4 (13%)	-	-	-
Estimation duration of infection before cART in days, median (IQR)	18 (14-22)	-	-	-
Plasma HIV RNA (log <sub>10</sub> copies/mL) at baseline, median (IQR)	6.10 (4.78-6.72)	-	-	-

a - 60% of clinical measures collected at latest follow-up (month 12 and month 18)

b - AHI(0) vs. CO(0) & AHI(24) vs. CO(0)

c - 40% of clinical measures collected at latest follow-up and/or baseline (month 0 and month 12)

## 3.2 Longitudinal Changes in Acute HIV

### *i. DTI Analysis*

BMLE models revealed statistically significant interaction effects between primary baseline predictors on changes in AHI participant MD metrics after adjusting for TIV. CD8 t-lymphocyte counts were associated with increasing MD metrics, suggesting that CD8 count at baseline significantly contributes to the MD global rate of change ( $p < 0.05$ ). This effect was present in the genu and splenium of the corpus callosum, the corona radiata, and the superior longitudinal fasciculus (**Figure 2A**). We identified no differences in any model when examining FA.

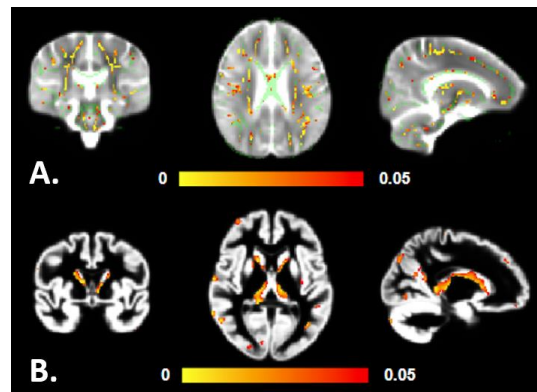


**Figure 2:** A. A p-value statistical map of significant voxel-wise group differences due to CD8 t-lymphocyte counts at baseline in increasing MD metrics of AHI participants followed longitudinally after adjusting for differences in TIV ( $p < 0.05$ ). DTI group template created with 0.2 threshold (in green) overlaid with significant changes (in red-yellow). B. A p-value statistical map of significant voxel-wise group differences (in red-yellow) due to CD8 t-lymphocyte counts at baseline in increased GM volumes of AHI participants followed longitudinally after adjusting for differences in TIV ( $p < 0.05$ ).

### *ii. Structural Analysis*

Conjugate VBM analysis of AHI participants, adjusted for age and TIV, demonstrated no significant differences between AHI (24) compared to AHI (0). In contrast, analysis of ROIs normalized with TIV and adjusted by age, revealed greater white matter volume of the corpus callosum, corroborated by large regional effect size ( $p < 0.01$ ,  $ES = -8.24$ ), among AHI (24)

compared to AHI (0) group (**Table 2-3**). Statistically significant group difference in the corpus callosum, normalized with TIV, persisted despite adjusting for both age and CD8 t-lymphocyte counts ( $p < 0.01$ ) (**Table 2**). BMLE models, however, revealed statistically significant interaction effects between primary baseline predictors on changes in AHI participant GM volumes after adjusting for TIV. CD8 t-lymphocyte counts were associated with increasing caudate and thalamus volumes (both  $p < 0.05$ ), suggesting that CD8 count at baseline significantly contributes to the GM volumetric rate of change (**Figure 2B**).

**Table 2:** Structural ROI analysis demonstrating significant regional differences in gray (GM) and white matter (WM) regions, including the corpus callosum (CC) and hippocampus. The table highlights changes observed in longitudinal comparison, AHI (0) vs. AHI (24), and changes by disease state, CO vs. AHI (24).

Structural Volume (ROI/TIV) $\beta$ (p-value)	$\beta_{AHI(0)-AHI(24)}$	$\beta_{CO-AHI(24)}$
	CC	Hippocampus
Age		
GM	-	-0.12 (0.05)
WM	0.64 (<0.01)	-
Age & CD8		
GM	-	-0.12 (0.05)
WM	0.63 (<0.01)	-
Age & Education		
GM	N/A	-0.19 (0.04)
WM	N/A	-

**Table 3:** Structural analysis of ROIs, normalized with TIV, demonstrating unadjusted differences in magnitude between groups, represented by calculated Cohen’s d effect size coefficients. The table highlights differences observed in longitudinal comparison, AHI (0) vs. AHI (24), and changes by disease state, CO vs. AHI (24).

Structural Volume Effect Size (ROI/TIV)	$\beta_{AHI(0) \cdot AHI(24)}$	$\beta_{CO \cdot AHI(24)}$
GM		
Frontal Lobe	-0.14	0.11
Temporal Lobe	-0.03	0.12
Caudate	0.03	-0.28
Nucleus Accumbens	0.28	0.07
Pallidum	0.23	0.14
Putamen	0.08	-0.19
Thalamus	0.01	0.20
Brainstem	<-0.01	0.10
Cerebellum	0.19	0.27
Hippocampus	0.13	0.49
Cortical Gray Matter	-0.11	0.24
WM		
Frontal Lobe	-0.07	-0.05
Temporal Lobe	-0.06	0.06
Brainstem	<-0.01	0.10
Corpus Callosum	-8.24	0.26
Cerebral White Matter	-0.02	0.09
Total White Matter	-0.02	0.08

### 3.3 Changes by Disease State: Healthy Controls vs. HIV Infected at 24 months

#### *i. DTI Analysis*

TBSS voxel-wise analysis of AHI participants compared to healthy controls demonstrated reduced FA measures of AHI after 24 months of cART compared to CO, linked across the corpus callosum, the corona radiata, and the superior longitudinal fasciculus (all  $p < 0.05$ ) in models adjusted for age and TIV (**Figure 3A**). We identified no differences in any model when examining MD. As a secondary analysis, age, TIV, and CD8 t-lymphocyte count, as a marker of inflammation, were adjusted for in model design. TBSS voxel-wise analysis revealed a preserved

finding of reduced FA of AHI (24) compared to CO, linked across corpus callosum, the corona radiata, and the superior longitudinal fasciculus (all  $p < 0.05$ ).

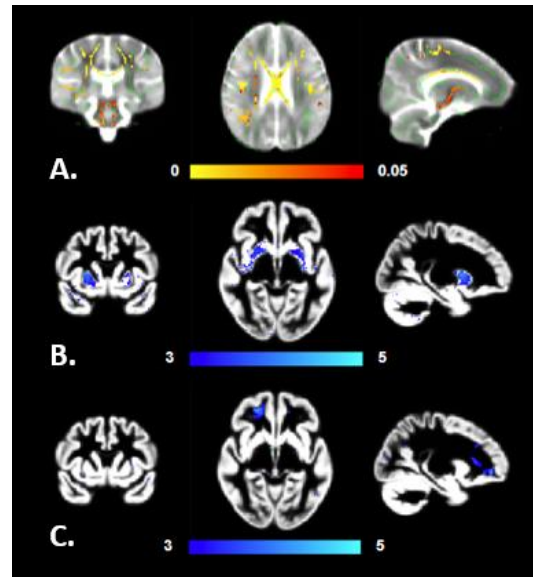


**Figure 3:** A. A p-value statistical map of significant voxel-wise group differences in FA metrics between CO and AHI (24) after adjusting for differences in age and TIV. DTI group template created with 0.2 threshold (in green) overlaid with significance (in red-yellow) representing significant differences ( $p < 0.05$ ). B. A t-score statistical map outside 3 standard deviations ( $\sigma$ ) between the CO and AHI (24) means in GM volumes after adjusting for differences in age and TIV. The group template overlaid with t-score (in blue-lightblue) represents significant differences ( $t = 3-5$ ). C. A t-score statistical map outside  $3\sigma$  between the CO and AHI (24) means in WM volumes after adjusting for differences in age and TIV. The group template overlaid with t-score (in blue-lightblue) represents significant differences ( $t = 3-5$ ).

### *ii. Structural Analysis*

VBM structural analysis, adjusted for age and TIV, revealed larger subcortical gray matter volumes close to statistical significance in both the putamen and the caudate ( $p < 0.10$ ;  $t > 3$ ), in AHI (24) compared to CO (**Figure 3B**). Analysis of ROIs normalized by TIV, however, revealed reduced gray matter hippocampal volumes, with medium effect size ( $p = 0.05$ ,  $ES = 0.49$ ) in the AHI (24) group relative to the CO group despite adjusting for age (**Table 2-3**). The same voxel-wise model design applied to white matter volumes demonstrated enlargement of the right frontal lobe

in the AHI (24) group relative to CO group ( $p < 0.05$ ;  $t > 3$ ) (**Figure 3C**). Analysis of ROIs normalized by TIV revealed no significant regional differences in white matter volumes after adjusting for age.

VBM analysis, adjusting for age, TIV, and CD8 t-lymphocyte counts did not resolve the same significant differences as models adjusting for age and TIV. ROI analysis normalized with TIV, however, demonstrated reduced gray matter hippocampal volumes ( $p = 0.05$ ) in the AHI (24) group relative to the CO group despite adjusting for age and CD8 counts. In white matter volumes, VBM analysis adjusted for age, TIV, and CD8 counts demonstrated enlargement of the right frontal lobe in the AHI (24) group relative to CO group close to statistical significance ( $p = 0.06$ ). Analysis of ROIs, normalized by TIV, revealed no significant regional differences after adjusting for age and CD8 counts.

### **3.4 Sensitivity Analysis**

A disproportionate number of AHI participants completed at least a bachelor's degree compared to the healthy controls (55% vs. 0%,  $p < 0.01$ ) (**Table 1**). BMLE models were used to consider whether baseline education in years and time impacted observed longitudinal AHI group differences in DTI metrics and structural volumes. TBSS and VBM group comparison models were used to consider whether differences of education in years impacted observed disease state group differences in DTI metrics and structural volumes, respectively.

#### *Longitudinal Analysis*

BMLE models were used to examine whether baseline education in years was associated with longitudinal changes in brain integrity during infection. Longitudinal analysis of AHI participants at AHI (0) compared to AHI (24) revealed that baseline education was associated with increased MD in the genu of the corpus callosum and the anterior corona radiata (both  $p < 0.05$ )



after adjusting for TIV. In gray matter volumes, baseline education was associated with a global increase in GM volumes. Specifically, increased frontal lobe, right temporal lobe, right caudate, right thalamus, cerebellum, and right hippocampus regions (all  $p < 0.05$ ) were observed in AHI participants followed longitudinally after adjusting for TIV.

#### *Changes By Disease State*

TBSS voxel-wise analysis revealed reduced FA in the AHI (24) group when compared to the CO group after adjusting for age, TIV, and education, linked across the corpus callosum, the corona radiata, and the left superior longitudinal fasciculus (all  $p < 0.05$ ). Conjugative VBM analysis revealed no significant differences in gray matter or white matter volumes of the AHI (24) group relative to the CO group. Comparative ROI analysis adjusting for age and education, however, revealed reduced gray matter hippocampal volumes ( $p = 0.04$ ) in the AHI (24) group relative to the CO group (**Table 2**).

## 4. Discussion

### 4.1 Major Findings

Our sample represents a novel cohort with neuroimaging data captured when cART was initiated in the first weeks of infection. We are not aware of any other cohort that has effectively examined longitudinal changes in brain integrity among individuals treated in the acute stage of infection. AHI participants were carefully selected to exclude confounding conditions and only include those individuals with paired imaging at both month 0 (baseline) and month 24 (two-years of cART followed longitudinally) who had successfully suppressed plasma virus. This approach strengthens the interpretations of longitudinal changes in brain volume and integrity despite successful viral suppression.

Differences of DTI metrics were observed in the AHI group followed longitudinally despite successful viral suppression. A statistically significant association between baseline CD8 t-lymphocyte count and an increase in MD metrics were observed after adjusting for age and TIV. As well, differences in structural volumes were reported. Baseline CD8 counts were associated with increasing GM volumes of AHI participants followed longitudinally after adjusting for TIV. In sensitivity analyses, we found that these changes were also associated with differences in baseline education in years.

Differences of DTI metrics in the AHI group were observed compared to healthy controls despite successful viral suppression. FA metrics demonstrated statistically significant reduction in AHI (24) compared to CO after adjusting for age and TIV, and this relationship persisted in models adjusted for age, TIV, and CD8 t-lymphocyte count. In sensitivity analyses, we also confirmed the finding in models adjusted for age, TIV, and education, given noted difference in educational attainment. Group differences between AHI (24) compared to CO were not associated with

observed differences in the amount of cytotoxic plasma CD8 t-lymphocyte cells (732 vs. 612,  $p=0.11$ ).

We conclude that despite successful viral suppression, physical changes affecting the brain integrity may continue to persist and develop over time. Structural analyses revealed enlarged gray and white matter volumes in AHI (24) compared to CO after adjusting for age, and age and CD8 t-lymphocyte count, which may be interpreted as an effect of infection, possibly enlargement associated with infiltration of immune cells in response to infection.

#### **4.2 Clinical Interpretations**

In a healthy state, water movement in the CNS is compartmentalized in intracellular and extracellular spaces (**Figure 4**). Adaptive immune cells are known to migrate to sites of infection to destroy foreign and unwanted microbes. Resident microglia also activate and flood axonal bundles with neurotoxic and neuroprotective factors.<sup>54,55</sup> As a result, both innate cellular and adaptive immune responses may cause chronic demyelination surrounding axonal bundles causing redirection of typically restricted extracellular flow. This may explain observed FA reduction in infected participants at follow-up relative to healthy controls.<sup>56</sup> Local immune responses may also lead to increased circulation of immune and subsequent scarring, which could cause impeded water movement. This may provide an explanation as to why we observed increased gray and white matter volumes in the longitudinally infected relative to healthy controls.

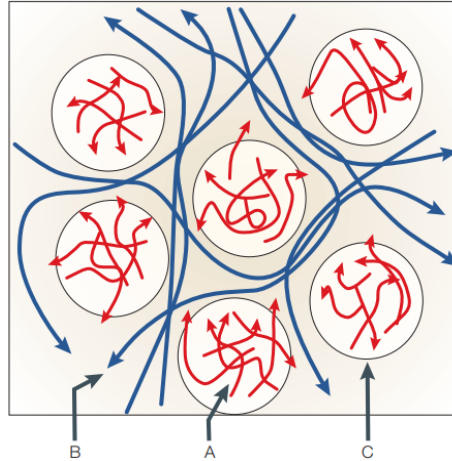


**Figure 4:** A visual representation of intracellular (in red) and extracellular (in blue) compartmentalized flow. Intracellular flow is bound by axonal or dendritic membranes. Extracellular flow is better approximated by a Gaussian displacement of water in extracellular spaces bound by cellular membranes of somas and glial cells.<sup>27</sup>

The association of baseline education and differential DTI longitudinal findings suggests there may be a relationship between the development of white matter tracts and educational attainment. As a result, educational differences may have been a contributor to observed differences in MD metrics. A recent study has identified the importance of educational attainment on white matter tract development (i.e. FA measures) in a cross-sectional design among late adolescents.<sup>57</sup> However, the longitudinal effects of educational attainment on healthy white matter tract development in early adulthood, which describes our participant group (approximately 20-30 years of age), let alone in a disease state, have yet to be examined.

Additionally, we cannot discount the fact that antiretroviral therapies, themselves, may contribute to observed differences in volumetric and DTI analysis. Many participants in our sample changed antiretroviral regimens over the course of 24 months. A subset of AHI participants received inconsistent antiretroviral regimen, switching from an EFV-based treatment, a non-nucleoside reverse transcriptase inhibitor (NNRTI), at month 0 baseline to a DTG-based treatment, an integrase strand transfer inhibitor (INSTI), at month 24 baseline (n=16). A single AHI

participant remained on an EFV-based treatment at both time points (n=1), while the remainder of considered AHI participants in our sample received a DTG-based treatment at both time points (n=14).

### **4.3 Exploratory Findings**

#### *Cross-sectional Differences by HIV Status at Baseline*

We repeated analysis done in our group as a confirmation of previous findings. TBSS voxel-wise analysis of healthy controls compared to the baseline AHI group showed reduced FA in AHI (0) compared to CO in the corpus callosum, the corona radiata, and the left superior fasciculus (all  $p < 0.05$ ) after adjusting for age and TIV. The same model demonstrated increased MD in the corpus callosum ( $p = 0.10$ ) close to statistical significance. VBM structural analysis, adjusted for differences in age and TIV, revealed enlarged gray matter volumes, namely the putamen, the caudate, and the nucleus accumbens (all  $p < 0.05$ ), in the infected group compared to the CO group. The AHI (0) group also exhibited larger white matter volumes, particularly in the frontal lobe, the temporal lobe, and the brainstem (all  $p < 0.05$ ) after adjusting for age and TIV.

#### *Differences in Treatment*

We addressed differences in treatment regimen by splitting AHI participants into two groups: participants who switched from EFV-based treatment to DTG-based treatment over the course of 24 months (n=16), and participants who remained on a DTG-based treatment at both time points (n=14). To limit variability, the single AHI participant who remained on EFV-based treatment at both time points was excluded from analysis. BMLE models adjusted for TIV showed two findings. First, CD8 t-lymphocyte count was significantly associated with a reduction in FA metrics in both groups. Second, this association was more pronounced in the group switching from

EFV-based to DTG-based treatment, suggesting that the treatment switch may have biased single group longitudinal findings.

#### **4.4 Limitations and Future Aims**

There were several limitations to this study. First, the sample size was small and lacked imaging data of healthy control participants followed longitudinally to month 24 follow-up. As such, BMLE models may have been particularly susceptible to inherent physiological or instrumental differences among individuals that could influence collected clinical and imaging data, respectively. As a result, statistical analysis may have captured these differences instead of differences due to longitudinal changes in brain integrity and volume. Continuation of this analysis would necessitate the inclusion of more AHI participants (expected  $n = 60$ ), as well as both chronic HIV (expected  $n = 40$ ) and healthy control groups (expected  $n = 40$ ) to represent relative changes of brain integrity and volume in later-stage disease and relative changes due to normal aging, respectively.

Due to the ongoing development and proven tolerance of second-generation antiretroviral therapies, a sizable proportion of early AHI participants switched from EFV-based to DTG-based antiretroviral therapy while more recently enrolled infected individuals began the DTG-based regimen.<sup>58</sup> The change in therapy among some participants hinders interpretation, since medical effects are possible. Future analysis will include further sensitivity analysis to investigate changes in brain structure and integrity within the HIV-infected group and determine whether choice of antiretroviral regimen biases single group findings.

Regional and functional variability may have also contributed to incongruent findings in structural ROIs when compared to voxel-wise analysis. Examining region of interest (e.g. functional units) differences involves interpreting mean values of often large groups of voxels,

which may overlook observed variabilities within the structure. Although analyzing subsections of regions may eliminate averaging out regional variability, diffusion among a group of voxels that represents diversely tortuous geometries inherently smooths away observed differences that may attribute to functional variability. Finer methods, such as functional analysis of diffusion tensor tract statistics (FADTTS), may better control for regional variance by implementing an additive spatial component in the analysis of diffusive motion. FADTTS considers the geometric orientation of diffusion signal within a well-defined tract as a parameter contributing to the voxel-wise value of diffusion metrics. Additionally, investigation of separable physical factors contributing to diffusive motion may be achieved by using more advanced diffusion imaging methods, like neurite orientation dispersion and density imaging (NODDI). NODDI uses an orientation-dispersion cylinder model and assumes there are three diffusion compartments in the brain (hindered, restricted, and free-water diffusion), to characterize angular variation and axon diameter as separate contributing factors in directional diffusivity. Thus, this model may be more effective at attributing changes in DTI indices to physical perturbations in neurite morphology and or neurite density.<sup>59,60</sup>

## 5. Conclusion

The analyses presented in this work are concerning that changes in brain integrity occur in HIV despite treatment with cART initiated in the very earliest stage of infection, suggesting the need for further development of adjuvant therapies for neuroprotection. We present proof of principle that such analyses can be accomplished and suggestions for findings that may emerge once our study reaches target enrollment numbers. Future work will also be powered to examine clinical and laboratory measures, such as neuropsychological testing performance, plasma biomarkers, and, potentially, cytokines measured in CSF to understand if they associate with any observed changes in brain integrity. This future work will provide greater clarity as to whether inflammation underlies anticipated observed differences in brain integrity.

In all, this study will overcome limitations in the existing literature where examination of DTI and volume abnormalities cannot exclude changes that occurred prior to the initiation of antiretroviral therapies since all participants in this study will start treatment within days of viral exposure. As well, our study will stand alone from prior studies that were completed among participants examined during primary HIV and will inform an early protective window (i.e. acute HIV), during which if treatment is initiated, changes noted in chronic HIV are mitigated. If early treatment ultimately proves to be neuroprotective in this novel cohort, findings may impact public health approaches encouraging the earliest possible treatment of HIV.



## References:

1. Kiertiburanakul S, Wongprasit P, Phuphuakrat A, Chotiprasitsakul D, Sungkanuparph S. Prevalence of HIV infection, access to HIV care, and response to antiretroviral therapy among partners of HIV-infected individuals in Thailand. *PLoS One*. 2018;13(6):1-12. doi:10.1371/journal.pone.0198654
2. O'Connor EE, Zeffiro TA, Zeffiro TA. Brain structural changes following HIV infection: Meta-analysis. *Am J Neuroradiol*. 2018;39(1):54-62. doi:10.3174/ajnr.A5432
3. Hakkers CS, Arends JE, Barth RE, Du Plessis S, Hoepelman AIM, Vink M. Review of functional MRI in HIV: effects of aging and medication. *J Neurovirol*. 2017;23(1):20-32. doi:10.1007/s13365-016-0483-y
4. Heaton RK, Clifford DB, Franklin DR, et al. HIV-associated neurocognitive disorders persist in the era of potent antiretroviral therapy: Charter Study. *Neurology*. 2010;75(23):2087-2096. doi:10.1212/WNL.0b013e318200d727
5. Tozzi V, Balestra P, Bellagamba R, et al. Persistence of Neuropsychologic Deficits Despite Long-Term Highly Active Antiretroviral Therapy in Patients Prevalence and Risk Factors. *J Acquir Immune Defic Syndr*. 2007;45(2):174-182.
6. Giancola ML, Lorenzini P, Balestra P, et al. Neuroactive Antiretroviral Drugs Do Not Influence Neurocognitive Performance in Less Advanced HIV-Infected Patients Responding to Highly Active Antiretroviral Therapy. *J Acquir Immune Defic Syndr*. 2006;41(3):332-337.
7. Simioni S, Cavassini M, Annoni J, et al. Cognitive dysfunction in HIV patients despite long-standing suppression of viremia. *AIDS*. 2010;24(November):1243-1250.

doi:10.1097/QAD.0b013e3283354a7b

8. Nightingale S, Winsto A, Letendre S, et al. Controversies in HIV-associated neurocognitive disorders. *Lancet Neurol.* 2015;13(11):1139-1151. doi:10.1016/S1474-4422(14)70137-1.Controversies
9. Milanini B, Ciccarelli N, Fabbiani M, et al. Cognitive reserve and neuropsychological functioning in older HIV-infected people. *J Neurovirol.* 2016;24(2):575-583. doi:10.1007/s13365-016-0426-7
10. Sacktor N, Hopkins J, Medical B, Neurology JH. Changing Clinical Phenotypes of HIV-Associated Neurocognitive Disorders Ned. *J Neurovirol.* 2018;24(2):141-145. doi:10.1007/s13365-017-0556-6.Changing
11. Fiebig EW, Wright DJ, Rawal BD, et al. Dynamics of HIV viremia and antibody seroconversion in plasma donors : implications for diagnosis and staging of primary HIV infection. *AIDS.* 2003;(March):1871-1879. doi:10.1097/01.aids.0000076308.76477.b8
12. Wawer MJ, Gray RH, Sewankambo NK, et al. Rates of HIV-1 Transmission per Coital Act, by Stage of HIV-1 Infection, in Rakai, Uganda. *J Infectious Diseases.* 2005;191:1403-1409.
13. Valcour V, Chalermchai T, Sailasuta N, et al. Central Nervous System Viral Invasion and Inflammation During Acute HIV Infection. *J Infectious Diseases.* 2012;206:275-282. doi:10.1093/infdis/jis326
14. Harezlak J, Buchtal S, Taylor M, Schifitto G, Zhong J. Persistence of HIV-Associated Cognitive Impairment, Inflammation and Neuronal Injury in era of Highly Active Antiretroviral Treatment. *AIDS.* 2015;25(5):625-633. doi:10.1097/QAD.0b013e3283427da7.Persistence
15. Sailasuta N, Ross W, Ananworanich J, et al. Change in Brain Magnetic Resonance

- Spectroscopy after Treatment during Acute HIV Infection. *PLoS One*. 2012;7(11). doi:10.1371/journal.pone.0049272
16. Kallianpur KJ, et al. Regional Brain Volumetric Changes Despite Two Years of Treatment Initiated During Acute HIV Infection. *Corresponding Author: Victor Valcour MD/PhD ; Abstract: CROI 2016*.
  17. Samboju V, Philippi CL, Chan P, et al. Structural and functional brain imaging in acute HIV. *NeuroImage Clin*. 2018;20(July):327-335. doi:10.1016/j.nicl.2018.07.024
  18. Hellmuth J, Fletcher JLK, Allen I, Krebs SJ, Slike B. Neurologic signs and symptoms frequently manifest in acute HIV infection. *Neurology*. 2016:1-8.
  19. Underwood J, Cole JH, Caan M, et al. Gray and White Matter Abnormalities in Treated Human Immunodeficiency Virus Disease and Their Relationship to Cognitive Function. *Clinical Infectious Diseases*. 2017;65. doi:10.1093/cid/cix301
  20. Ances BM, Ortega M, Vaida F, Heaps J, Paul R. Independent effects of HIV, aging, and HAART on brain volumetric measures. *J Acquir Immune Defic Syndr*. 2012;59(5):469-477. doi:10.1097/QAI.0b013e318249db17
  21. Jahanshad N, Valcour VG, Ba TMN, et al. Disrupted brain networks in the aging HIV + population. *Brain Connectivity* :2012;(310):1-23.
  22. Su T, Caan MWA, Wit FWNM, et al. White matter structure alterations in HIV-1-infected men with sustained suppression of viraemia on treatment. *AIDS*. 2016;30(2):311-322. doi:10.1097/QAD.0000000000000945
  23. Chang K, Premeaux TA, Cobigo Y, et al. Virally Suppressed HIV-Infected Individuals Short Title : Biomarkers Link to DTI in Suppressed HIV. *Corresponding Author: Victor Valcour MD PhD; Abstract: CROI 2019*.

24. Ragin AB, Wu Y, Gao Y, et al. Brain alterations within the first 100 days of HIV infection. *Ann Clin Transl Neurol.* 2015;2(1):12-21. doi:10.1002/acn3.136
25. Wendelken, LA, Jahanshad, N, Rosen, HJ, Busovaca, E, Allen, I, Coppola, G, Adams, C, Rankin, KP, Milanini, B, Clifford, K, Wojta, K, Nir, TM, Gutman, BA, Thompson, PM, Valcour V. ApoE  $\epsilon$ 4 is Associated with Cognition, Brain Integrity and Atrophy in HIV Over Age 60. 2016;73(4):426-432. *J Acquir Immune Defic Syndr.* doi:10.1002/jmri.25711.PET/MRI
26. Alexander AL, Lee JE, Lazar M, Field AS. Diffusion Tensor Imaging of the Brain. *Neurotherapeutics.* 2008;4(3):316-329.
27. Le Bihan D. Looking into the functional architecture of the brain with diffusion MRI. *Int Nature Reviews: Neuroscience.* 2003;4:469-480. doi:10.1016/j.ics.2006.04.006
28. Basser P, Mattiello J, LeBihan D. Estimation of Effective Self-Diffusion Tensor from the NMR Spin Echo. *J Magnetic Resonance.* 1994:247-254.
29. Stejskal EO, Tanner JE. Spin diffusion measurements: Spin echoes in the presence of a time-dependent field gradient. *J Chem Phys.* 1965;42(1):288-292. doi:10.1063/1.1695690
30. Veraart J, Novikov DS, Christiaens D, Ades-Aron B, Sijbers J, Fieremans E. Denoising of diffusion MRI using random matrix theory. *Neuroimage.* 2016;142:394-406. doi:10.1016/j.neuroimage.2016.08.016
31. Jenkinson M, Bannister P, Brady M, Smith S. Improved optimization for the robust and accurate linear registration and motion correction of brain images. *Neuroimage.* 2002;17(2):825-841. doi:10.1006/nimg.2002.1132
32. Otsu N. A Threshold Selection Method from Gray-Level Histograms. *IEEE Trans Syst Man Cybern.* 1979;9(1):62-66. doi:10.1109/TSMC.1979.4310076

33. Garyfallidis E, Brett M, Amirbekian B, et al. Dipy, a library for the analysis of diffusion MRI data. *Front Neuroinform.* 2014;8(February):1-17. doi:10.3389/fninf.2014.00008
34. Andersson JLR, Sotiropoulos SN. An integrated approach to correction for off-resonance effects and subject movement in diffusion MR imaging. *Neuroimage.* 2016;125:1063-1078. doi:10.1016/j.neuroimage.2015.10.019
35. Basser PJ, Pierpaoli C. Microstructural and physiological features of tissues elucidated by quantitative-diffusion-tensor MRI. *J Magn Reson - Ser B.* 1996;111(3):209-219. doi:10.1006/jmrb.1996.0086
36. Ashburner J, Friston KJ. Unified segmentation. *Neuroimage.* 2005;26(3):839-851. doi:10.1016/j.neuroimage.2005.02.018
37. Ashburner J, Ridgway GR. Symmetric diffeomorphic modeling of longitudinal structural MRI. *Front Neurosci.* 2013;6(FEB):1-19. doi:10.3389/fnins.2012.00197
38. Ziegler G, Penny WD, Ridgway GR, Ourselin S, Friston KJ. Estimating anatomical trajectories with Bayesian mixed-effects modeling. *Neuroimage.* 2015;121:51-68. doi:10.1016/j.neuroimage.2015.06.094
39. Ashburner J, Friston KJ. Diffeomorphic registration using geodesic shooting and Gauss-Newton optimisation. *Neuroimage.* 2011;55(3):954-967. doi:10.1016/j.neuroimage.2010.12.049
40. Fonov, V, Evans, A.C., Botteron, K, Almlí, C.R., McKinstry, R.C., Collins DC. Unbiased Average Age-Appropriate Atlases for Pediatric Studies. *Neuroimage.* 2011;54(1):313-327. doi:10.1371/journal.pone.0178059
41. Ashburner J, Friston KJ. Voxel-based morphometry - The methods. *Neuroimage.* 2000;11(6):805-821. doi:10.1006/nimg.2000.0582

42. Smith SM, Jenkinson M, Johansen-Berg H, et al. Tract-based spatial statistics: voxelwise analysis of multi-subject diffusion data. *Neuroimage*. 2006;31(4):1487-1505. doi:10.1016/j.neuroimage.2006.02.024
43. Whitwell JL, Crum WR, Watt HC, Fox NC. Normalization of Cerebral Volumes by Use of Intracranial Volume: Implications for Longitudinal Quantitative MR Imaging. *Am J Neuroradiol*. 2014;22(September):1483-1489.
44. Takao H, Hayashi N, Ohtomo K. Sex dimorphism in the white matter: Fractional anisotropy and brain size. *J Magn Reson Imaging*. 2014;39(4):917-923. doi:10.1002/jmri.24225
45. Kanaan RA, Allin M, Picchioni M, et al. Gender differences in white matter microstructure. *PLoS One*. 2012;7(6):e38272. doi:10.1371/journal.pone.0038272
46. Inano S, Takao H, Hayashi N, Abe O, Ohtomo K. Effects of age and gender on white matter integrity. *Am J Neuroradiol*. 2011;32(11):2103-2109. doi:10.3174/ajnr.A2785
47. Smith SM, Johansen-Berg H, Jenkinson M, et al. Acquisition and voxelwise analysis of multi-subject diffusion data with tract-based spatial statistics. *Nat Protoc*. 2007;2(3):499-503. doi:10.1038/nprot.2007.45
48. Smith SM, Jenkinson M, Woolrich MW, et al. Advances in functional and structural MR image analysis and implementation as FSL. *Neuroimage*. 2004;23(SUPPL. 1):208-219. doi:10.1016/j.neuroimage.2004.07.051
49. Winkler AM, Ridgway GR, Webster MA, Smith SM, Nichols TE. Permutation inference for the general linear model. *Neuroimage*. 2014;92:381-397. doi:10.1016/j.neuroimage.2014.01.060
50. Kranick SM, Nath A. Neurologic Complications of HIV-1 Infection and Its Treatment in the Era of Antiretroviral Therapy. *Continuum Lifelong Learning Neurology*. 2012;18(6):

- 1319-1337.
51. Desikan RS, Ségonne F, Fischl B, et al. An automated labeling system for subdividing the human cerebral cortex on MRI scans into gyral based regions of interest. *Neuroimage*. 2006;31(3):968-980. doi:10.1016/j.neuroimage.2006.01.021
  52. Chiang MC, Dutton RA, Hayashi KM, et al. 3D pattern of brain atrophy in HIV/AIDS visualized using tensor-based morphometry. *Neuroimage*. 2007;34(1):44-60. doi:10.1016/j.neuroimage.2006.08.030
  53. Clifford KM, Samboju V, Cobigo Y, et al. Progressive Brain Atrophy Despite Persistent Viral Suppression in HIV Over Age 60. *J Acquir Immune Defic Syndr*. 2017;76(3):289-297. doi:10.1097/QAI.0000000000001489
  54. Schwartz M, Kipnis J, Rivest S, Prat A. How do immune cells support and shape the brain in health, disease, and aging? *J Neurosci*. 2013;33(45):17587-17596. doi:10.1523/JNEUROSCI.3241-13.2013
  55. He J, Chen Y, Farzan M, et al. CCR3 and CCR5 are co-receptors for HIV-1 infection of microglia. 1997;385(13):645-649.
  56. Rolls A, Shechter R, Schwartz M. The bright side of the glial scar in CNS repair. *Nature Reviews: Neuroscience*. 2009;10(March):235-241.
  57. Noble KG, Korgaonkar MS, Grieve SM, Brickman AM. Higher Education is an Age-Independent Predictor of White Matter Integrity and Cognitive Control in Late Adolescence. *Dev Sci*. 2013;16(5):653-664. doi:10.1111/desc.12077
  58. Goh OQ, Colby DJ, et al. Switch to dolutegravir is well tolerated in Thais with HIV infection. *J Int AIDS Soc*. 2019;22(7):1-8. doi:10.1002/jia2.25324
  59. Zhang H, Schneider T, Wheeler-Kingshott CA, Alexander DC. NODDI: Practical in vivo

neurite orientation dispersion and density imaging of the human brain. *Neuroimage*. 2012;61(4):1000-1016. doi:10.1016/j.neuroimage.2012.03.072

60. Zhang H, Hubbard PL, Parker GJM, Alexander DC. Axon diameter mapping in the presence of orientation dispersion with diffusion MRI. *Neuroimage*. 2011;56(3):1301-1315. doi:10.1016/j.neuroimage.2011.01.084



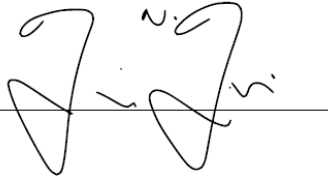
**Publishing Agreement**

*It is the policy of the University to encourage the distribution of all theses, dissertations, and manuscripts. Copies of all UCSF theses, dissertations, and manuscripts will be routed to the library via the Graduate Division. The library will make all theses, dissertations, and manuscripts accessible to the public and will preserve these to the best of their abilities, in perpetuity.*

***Please sign the following statement:***

*I hereby grant permission to the Graduate Division of the University of California, San Francisco to release copies of my thesis, dissertation, or manuscript to the Campus Library to provide access and preservation, in whole or in part, in perpetuity.*

\_\_\_\_\_  
Author Signature

A handwritten signature in black ink, appearing to be 'J. N. ...', written over a horizontal line.

\_\_\_\_\_  
August 30, 2019  
Date